Exciton center-of-mass dispersion in semiconductor quantum wells

Adriana L. C. Triques and José A. Brum
Instituto de Física Gleb Wataghin, DFESCM, Universidade Estadual de Campinas, 13083-970 Campinas (SP), Brazil
(Received 9 January 1997)

We discuss the results of the calculation of the exciton center-of-mass dispersion in a semiconductor quantum well. Strong nonparabolicity arises due to the coupling among the excitons related to the heavy and light holes. We consider the effects of the coupling in the exciton dynamics by calculating the exciton average mass and spin. [S0163-1829(97)06224-3]

I. INTRODUCTION

The exciton is the lowest-energy excited state of a pure semiconductor crystal, built upon the excitation of an electron from the valence band to the conduction band. The Coulomb interaction among the valence and conduction electrons affects not only the band-edge electronic states, but also states above the energy gap.[1] This strongly influences the optical properties of the system: Strong excitonic peaks can be detected on the threshold of optical absorption spectra, as well as an enhancement on the absorption of the continuum states in semiconductor crystals.[2,3] The excitons show an energy dispersion which is directly related to the electron and hole dispersions and greatly influences the dynamics of the system excitations.[4–6]

In many of the bulk semiconductors of interest, the exciton binding energy is weak (5 meV for GaAs) and the problem can be described within the effective-mass approximation (Wannier exciton).[7] The effective mass theory for the Wannier excitons in the case of degenerate electronic bands was discussed by Dresselhaus.[8] In his work, the absence of a well-defined exciton center-of-mass (c.m.) transformation arising from the degenerate nature of the valence bands is clearly shown. Accounting for this fact, Altarelli and Lipari[4] calculated the exciton-c.m. dispersion for direct- and indirect-gap bulk semiconductors with degenerate bands. In their calculations, a general c.m. transformation is introduced to achieve formal simplicity and numerical accuracy for the solutions. The results show that the degeneracy and coupling of the upper valence bands causes a nonparabolic and anisotropic exciton-c.m. dispersion. Éfros and Gelmont[5] and Gelmont *et al.*[6] analyzed the shape of the exciton-c.m. dispersion near the Γ point. They predicted that, under certain conditions, the minimum of the exciton-c.m. dispersion may be off the Γ point. This is an important aspect since in this case the exciton would relax to states which do not couple with the electromagnetic field, delaying significantly the exciton recombination.

In semiconductor quantum wells (QW's), the spatial confinement of electrons and holes causes the enhancement of the exciton binding energy and allows it to effectively dominate the optical properties even at room temperatures.[3,9–12] The QW potential breaks the translational symmetry along the growth axis, and several new features appear in the exciton behavior. In particular, the QW breaks the valence-band degeneracy at $\vec{k}_h=0$. As a consequence, heavy- and light-hole excitons are formed. For QW widths comparable to the exciton radius, the QW confinement dominates over the exciton binding energy and it is reasonable to work with the concept of a quasi-two-dimensional (quasi-2D) exciton. Due to the energy separation among the heavy- and light-hole QW states, a parabolic dispersion for the hole states was initially considered for the quasi-2D exciton.[13,14] In this description, the in-plane hole mass reversal is responsible for the higher binding energy for the light-hole exciton in comparison to the heavy-hole exciton.[13,14] Altarelli[15] considered the coupling among the heavy- and light-hole states in the in-plane hole dispersion for the QW semiconductors. He predicted a strong nonparabolicity for the hole states, in particular for the ground–light-hole state which may show an in-plane dispersion with a camel-back shape, that is, a minimum in the in-plane dispersion off the zone center. These effects were introduced in the excitonic problem by Chan[16] and Bauer and Ando.[17] The first result is an enhancement in the exciton binding energy of the order of 10%–20%. A more spectacular effect is the coupling among the quasi-2D excitons with different angular momenta. As a consequence of the coupling, part of the oscillator strength of the s-like excitons is transferred to the higher-angular-momentum excitons formed by holes from different J_z values, which become, then, optically active. Since the coupling among these excitons is relatively weak, these effects are more significant when the excitons are nearly resonant. High-quality samples have shown a great number of new absorption lines due to these effects which can be monitored through the application of external fields such as an electric field[18,19] or a magnetic field[20] along the growth direction as well as stress fields applied perpendicularly to the growth direction.[21] Both effects, the enhancement of the binding energy and the exchange of oscillator strengths among excitons with different envelope function angular momenta, are relatively weak effects and require high-quality samples for their observation. This is understandable since they are related to the relative motion which is mainly affected by the lighter mass, that is, the electron mass.

The understanding of the exciton-c.m. dispersion is of fundamental importance in QW's. The photoluminescence spectra and their temporal evolution are determined by the excitonic properties and by the exciton formation and relaxation dynamics.[22,23] The exciton formation and subsequent relaxation from $\vec{K}_{\text{c.m.}}\neq 0$ to $\vec{K}_{\text{c.m.}}=0$ states,[24–27] its coupling to the electromagnetic field (exciton-polariton),[28–30] exci-

tonic indirect transitions,[31] and the exciton spin relaxation[32,33] in semiconductor heterostructures are some of the problems of current interest that depend directly on the exciton-c.m. dispersion. Recently, a great deal of effort has been devoted to the understanding of the exciton diffusion and localization in the plane of the QW interfaces due to their roughness.[34–36] In some cases, the control of the growth of these roughnesses may be used as a tool to achieve lateral confinement.[37,38] The exciton diffusion and eventual localization in the interfaces are strongly dependent on the exciton in-plane mass. The recent development of spectroscopic techniques with high temporal and spatial resolution allows the study of these processes. It is of fundamental importance, therefore, to evaluate the exciton-c.m. dispersion features in order to acquire a clear picture of these processes.

If we consider the in-plane exciton-c.m. dispersion, we should expect a strong influence of the valence-band mixing, contrary to relative motion effects, since now the heavier mass dominates the kinetics. Actually, in a first approach, it is expected that most of the features observed in the in-plane hole dispersion would be present for the in-plane exciton dispersion. These effects may, however, be smoothed out by the electronic parabolic mass. This problem was discussed for the first time in QW's by Chu *et al.*[39] considering the strongly strained QW's. They predicted that InGaAs QW's under uniaxial stress may present an indirect exciton. Their model, however, does not contemplate the whole coupling among excitons with different in-plane symmetries. This situation was experimentally observed by Michler *et al.*[31] for intrinsically strained materials. Exciton-c.m. dispersion was also considered in indirect gap heterostructures.[40]

In this paper we present results of the calculation of the in-plane exciton center-of-mass (c.m.) dispersion for GaAs/AlGaAs quantum well systems in the effective-mass approximation, taking into account valence-band mixing. Preliminary reports of our model were presented before,[41] focusing in particular on the strained materials as the one studied by Michler *et al.*[31] Here we present the model and discuss the general results. The mixing is reflected in a remarkable nonparabolicity of the exciton-c.m. dispersion. A camel-back structure for the light-hole exciton may be observed and distinguished at least for QW's wider than 150 Å. We also analyze the in-plane warping and the effect of an external electric field on the dispersion. Finally, we discuss the exciton spin mixing in the QW, tracing the dependence of the average spin value on the exciton-c.m. wave vector $\vec{K}_{\text{c.m.}}$. This gives insight into the influence of the exciton mixing in the exciton spin relaxation process that is undergone during exciton formation and relaxation to $\vec{K}_{\text{c.m.}}=0$.

The paper is organized as follows. In Sec. II, the model is presented. Section III is reserved for the results and discussions, focusing the general aspects (Sec. III A), the effect of an electric field (Sec. III B), and the exciton spin (Sec. III C). Section IV contains the summary and concluding remarks.

II. THEORETICAL APPROACH

We want to describe the exciton-c.m. dispersion in a semiconductor QW system including valence-band mixing. The theoretical approach follows the effective-mass approximation in the Wannier exciton limit.[7] We apply our model to GaAs/$Ga_{1-x}Al_xAs$ QW's. The conduction-band nonparabolicity is neglected since it is not an important contribution to the exciton binding energy in these systems. The valence bands are described by the Luttinger Hamiltonian.[42] The split-off band is well separated in energy from the heavy- and light-hole bands for the exciton states considered here and it is not included in the Luttinger Hamiltonian. The exchange interaction is neglected in our calculations. We also neglect the difference in the effective parameters between the two materials and assume those of the GaAs bulk. The exciton states are constructed by the direct product of the conduction electron and the valence hole states. We assume that the kinetics along the growth direction (z direction) is dominated by the QW confinement. We therefore apply a c.m. transformation only for the in-plane coordinates:

$$\vec{\rho}=(x_e-x_h,y_e-y_h,0) \tag{1}$$

and

$$\vec{R}_{\text{c.m.}}=\alpha(x_e,y_e,0)+\beta(x_h,y_h,0). \tag{2}$$

The valence states are written in the $|J,J_z\rangle$ basis. The exciton Hamiltonian is

$$\mathbf{H}_{\text{exc}}=H_e(z_e)\mathbf{1}+\mathbf{H}_1(z_h,\vec{\rho})+\mathbf{H}_2(z_h,\vec{\rho},\vec{R}_{\text{c.m.}}) + V_C(z_e-z_h,\rho)\mathbf{1}, \tag{3}$$

where

$$H_e(z_e)=E_g-\frac{\hbar^2}{2m_e}\frac{\partial^2}{\partial z_e^2}+V_eY\left(z_e^2-\frac{L^2}{4}\right), \tag{4}$$

$$\mathbf{H}_1(z_h,\vec{\rho})=\begin{bmatrix} a_+ & c & b & 0\\ c^* & a_- & 0 & -b\\ b^* & 0 & a_- & c\\ 0 & -b^* & c^* & a_+\end{bmatrix}, \tag{5}$$

with

$$a_\pm=\frac{\hbar^2}{2m_0}(-\gamma_1\mp 2\gamma_2)\frac{\partial^2}{\partial z_h^2}+V_hY\left(z_h^2-\frac{L^2}{4}\right) -\frac{\hbar^2}{2m_0}\left(\frac{m_0}{m_e}+\gamma_1\pm\gamma_2\right)\left(\frac{\partial^2}{\partial x^2}+\frac{\partial^2}{\partial y^2}\right), \tag{6}$$

$$b=-\left(\frac{\sqrt{3}\hbar^2}{m_0}\right)\gamma_3\frac{\partial}{\partial z_h}\left(\frac{\partial}{\partial x}-i\frac{\partial}{\partial y}\right), \tag{7}$$

$$c=-\left(\frac{\sqrt{3}\hbar^2}{2m_0}\right)\left[\gamma_2\left(\frac{\partial^2}{\partial x^2}-\frac{\partial^2}{\partial y^2}\right)-2i\gamma_3\frac{\partial^2}{\partial x\partial y}\right], \tag{8}$$

$$\mathbf{H}_2(z_h,\vec{\rho},\vec{R}_{\text{c.m.}})=\begin{bmatrix} A_+ & C & B & 0\\ C^* & A_- & 0 & -B\\ B^* & 0 & A_- & C\\ 0 & -B^* & C^* & A_+\end{bmatrix}, \tag{9}$$

with

$$A_{\pm}=-\frac{\hbar^2}{2m_0}\left(\alpha^2\frac{m_0}{m_e}+\beta^2(\gamma_1\pm\gamma_2)\right)\left(\frac{\partial^2}{\partial X_{\text{c.m.}}^2}+\frac{\partial^2}{\partial Y_{\text{c.m.}}^2}\right)-\frac{\hbar^2}{m_0}\left(\alpha\frac{m_0}{m_e}-\beta(\gamma_1\pm\gamma_2)\right)\left(\frac{\partial^2}{\partial x\,\partial X_{\text{c.m.}}}+\frac{\partial^2}{\partial y\,\partial X_{\text{c.m.}}}\right), \tag{10}$$

$$B=\left(\frac{\sqrt{3}\hbar^2}{m_0}\right)\beta\gamma_3\frac{\partial}{\partial z_h}\left(\frac{\partial}{\partial X_{\text{c.m.}}}-i\frac{\partial}{\partial Y_{\text{c.m.}}}\right), \tag{11}$$

$$C=-\left(\frac{\sqrt{3}\hbar^2}{2m_0}\right)(\gamma_2+\gamma_3)\left[\beta^2\left(\frac{\partial}{\partial X_{\text{c.m.}}}-i\frac{\partial}{\partial Y_{\text{c.m.}}}\right)^2-2\beta\left(\frac{\partial}{\partial X_{\text{c.m.}}}-i\frac{\partial}{\partial Y_{\text{c.m.}}}\right)\left(\frac{\partial}{\partial x}-i\frac{\partial}{\partial y}\right)\right]+(\gamma_2-\gamma_3)\times\left[\beta^2\left(\frac{\partial}{\partial X_{\text{c.m.}}}+i\frac{\partial}{\partial Y_{\text{c.m.}}}\right)^2-2\beta\left(\frac{\partial}{\partial X_{\text{c.m.}}}+i\frac{\partial}{\partial Y_{\text{c.m.}}}\right)\times\left(\frac{\partial}{\partial x}+i\frac{\partial}{\partial y}\right)\right], \tag{12}$$

$$V_C(z_e-z_h,\rho)=\frac{-e^2}{\kappa\sqrt{(z_e-z_h)^2+\rho^2}}. \tag{13}$$

1 is a unitary 4×4 matrix. $Y(x)$ is the step function [$Y(x)=0$ if $x<0$, $Y(x)=1$ otherwise]. $V_e=\Delta E_g Q_e$ and $V_h=\Delta E_g(1-Q_e)$, where Q_e is the conduction-band offset and ΔE_g is the gap discontinuity at the interface. m_e is the electron effective mass in the conduction band, γ_1, γ_2, and γ_3 are the Luttinger parameters, and the other constants have their usual definitions. The Hamiltonian is written with the basis $|s_e\rangle\otimes|J,J_z\rangle$ in the following order: $|\pm1/2\rangle\otimes|3/2,+3/2\rangle$, $|\pm1/2\rangle\otimes|3/2,-1/2\rangle$, $|\pm1/2\rangle\otimes|3/2,+1/2\rangle$, $|\pm1/2\rangle\otimes|3/2,-3/2\rangle$.

The off-diagonal terms of the Luttinger Hamiltonian, which couple the heavy- and light-hole states for $\mathbf{k}_h\neq0$, are responsible for the coupling among the relative and c.m. motions of the heavy- and light-hole excitons. This implies that there is no longer a simple c.m. transformation for the coupled exciton problem. In other words, there is no preferable choice for α and β in Eq. (2). We impose $\alpha+\beta=1$ so that the Jacobian of the transformation is unitary.[4] The eigenstates are independent of the particular choice of the parameters α and β. The variational wave function is

$$\vec{\Psi}_{\text{exc}}(z_e,z_h,\vec{\rho},\vec{R}_{\text{c.m.}})=f_p(z_e)\begin{bmatrix}\Sigma_{m,j,\lambda_j}c^1_{m,j,\lambda_j}g_m^+(z_h)\Psi_j(\rho,\theta,\lambda_j)\\ \Sigma_{n,j,\lambda_j}c^2_{n,j,\lambda_j}g_n^-(z_h)\Psi_j(\rho,\theta,\lambda_j)\\ \Sigma_{n,j,\lambda_j}c^3_{n,j,\lambda_j}g_n^-(z_h)\Psi_j(\rho,\theta,\lambda_j)\\ \Sigma_{m,j,\lambda_j}c^4_{m,j,\lambda_j}g_m^+(z_h)\Psi_j(\rho,\theta,\lambda_j)\end{bmatrix}\times\frac{\exp[i\vec{K}_{\text{c.m.}}\cdot\vec{R}_{\text{c.m.}}]}{\sqrt{S}}, \tag{14}$$

with

$$H_e(ze)f_p(z_e)=e_pf_p(z_e), \tag{15}$$

$$\left[\frac{-\hbar^2}{2m_0}(\gamma_1-2\gamma_2)\frac{\partial^2}{\partial z_h^2}+V_hY\left(z_h-\frac{L^2}{4}\right)\right]g_m^+(z_h)=hh_mg_m^+(z_h), \tag{16}$$

$$\left[\frac{-\hbar^2}{2m_0}(\gamma_1+2\gamma_2)\frac{\partial^2}{\partial z_h^2}+V_hY\left(z_h-\frac{L^2}{4}\right)\right]g_n^-(z_h)=lh_ng_n^-(z_h). \tag{17}$$

S is the sample area. The $\Psi_j(\rho,\theta,\lambda_j)$ are the in-plane relative motion wave functions. We choose them as a set of 2D in-plane hydrogeniclike wave functions:

$$\Psi_s(\rho,\theta,\lambda_s)=N_{s\lambda_s}\exp\left(-\frac{\rho}{\lambda_s}\right), \tag{18}$$

$$\Psi_{\pm p}(\rho,\theta,\lambda_p)=N_{p\lambda_p}\exp\left(-\frac{\rho}{\lambda_p}\pm i\theta\right), \tag{19}$$

$$\Psi_{\pm d}(\rho,\theta,\lambda_d)=N_{d\lambda_d}\rho^2\exp\left(-\frac{\rho}{\lambda_d}\pm2i\theta\right), \tag{20}$$

$$\Psi_{\pm f}(\rho,\theta,\lambda_f)=N_{f\lambda_f}\rho^3\exp\left(-\frac{\rho}{\lambda_f}\pm3i\theta\right). \tag{21}$$

The parameters λ_j are chosen in geometric progression within the range of 10–1000 Å. The c^k_{m,j,λ_j}'s are the variational parameters. The eigenvalues and eigenfunctions are obtained by minimizing the expectation value of the Hamiltonian, $\langle\vec{\Psi}_{\text{exc}}|\mathbf{H}_{\text{exc}}|\vec{\Psi}_{\text{exc}}\rangle$, as a function of the parameters c^k_{m,j,λ_j}'s. The resulting generalized eigenvalue problem is then numerically diagonalized.

Our basis set well describes the ground state and a few excited exciton states with great accuracy. The continuum exciton states are present only through a set of discrete states lying within the energy range of the continuum states. Although this is a poor description of those states, this set is flexible enough to give the proper contribution for the bound states of their coupling with the continuum states.[43] We neglect the coupling by the Coulomb interaction among the exciton states originating from different electron and hole subbands. This coupling is important only for very narrow or very large wells. Another situation where this coupling produces significant results is when a bound exciton from higher subbands lies within the continuum of excitons associated with lower subbands. In this case, the bound exciton is actually a Fano resonance.[44–47] Although this situation is often the case in real samples, these effects are weak and require high-quality samples to be observed.[46] We concentrate here in the dispersion of the bound excitons and do not analyze the resonance problem.

For symmetric QW's it is possible to separate the Hamiltonian into two uncoupled blocks, each one representing one of the parities.[48] The two general wave functions are

$$\vec{\Psi}^{\uparrow}_{\rm exc}(z_e,z_h,\vec{\rho},\vec{R}_{\rm c.m.})=f_p(z_e)\begin{bmatrix}\sum_{m({\rm even}),j,\lambda_j} c^1_{m,j,\lambda_j} g^+_m(z_h)\Psi_j(\vec{\rho},\lambda_j)\\ \sum_{n({\rm even}),j,\lambda_j} c^2_{n,j,\lambda_j} g^-_n(z_h)\Psi_j(\vec{\rho},\lambda_j)\\ \sum_{n({\rm odd}),j,\lambda_j} c^3_{n,j,\lambda_j} g^-_n(z_h)\Psi_j(\vec{\rho},\lambda_j)\\ \sum_{m({\rm odd}),j,\lambda_j} c^4_{m,j,\lambda_j} g^+_m(z_h)\Psi_j(\vec{\rho},\lambda_j)\end{bmatrix}\frac{\exp[i\vec{K}_{\rm c.m.}\cdot\vec{R}_{\rm c.m.}]}{\sqrt{S}} \tag{22}$$

and

$$\vec{\Psi}^{\downarrow}_{\rm exc}(z_e,z_h,\vec{\rho},\vec{R}_{\rm c.m.})=f_p(z_e)\begin{bmatrix}\sum_{m({\rm odd}),j,\lambda_j} c^1_{m,j,\lambda_j} g^+_m(z_h)\Psi_j(\vec{\rho},\lambda_j)\\ \sum_{n({\rm odd}),j,\lambda_j} c^2_{n,j,\lambda_j} g^-_n(z_h)\Psi_j(\vec{\rho},\lambda_j)\\ \sum_{n({\rm even}),j,\lambda_j} c^3_{n,j,\lambda_j} g^-_n(z_h)\Psi_j(\vec{\rho},\lambda_j)\\ \sum_{m({\rm even}),j,\lambda_j} c^4_{m,j,\lambda_j} g^+_m(z_h)\Psi_j(\vec{\rho},\lambda_j)\end{bmatrix}\frac{\exp[i\vec{K}_{\rm c.m.}\cdot\vec{R}_{\rm c.m.}]}{\sqrt{S}}, \tag{23}$$

where the arrow indicates the parity quantum number. Each wave function [Eqs. (22) and (23)] corresponds to two degenerate sets of solutions, related to the two possible choices for the electron spin. Referring to the spin of the ground state of the uncoupled heavy-hole and light-hole excitons, $e_1-hh_1{:}1s$ and $e_1-lh_1{:}1s$ excitons, respectively, the wave function of Eq. (22) describes, independently, the spin states

$$S^{hh}_{\rm exc}=2 \quad (s_e=\tfrac{1}{2},J_z=\tfrac{3}{2}), \tag{24}$$

$$S^{lh}_{\rm exc}=0 \quad (s_e=\tfrac{1}{2},J_z=-\tfrac{1}{2}) \tag{25}$$

or

$$S^{hh}_{\rm exc}=1 \quad (s_e=-\tfrac{1}{2},J_z=\tfrac{3}{2}), \tag{26}$$

$$S^{lh}_{\rm exc}=-1 \quad (s_e=-\tfrac{1}{2},J_z=-\tfrac{1}{2}), \tag{27}$$

while Eq. (23) describes the spin states

$$S^{hh}_{\rm exc}=-1 \quad (s_e=\tfrac{1}{2},J_z=-\tfrac{3}{2}), \tag{28}$$

$$S^{lh}_{\rm exc}=1 \quad (s_e=\tfrac{1}{2},J_z=\tfrac{1}{2}) \tag{29}$$

or

$$S^{hh}_{\rm exc}=-2 \quad (s_e=-\tfrac{1}{2},J_z=-\tfrac{3}{2}), \tag{30}$$

$$S^{lh}_{\rm exc}=0 \quad (s_e=-\tfrac{1}{2},J_z=\tfrac{1}{2}). \tag{31}$$

The exciton states with spin $S_{\rm exc}=\pm 2$ are not optically active and are called dark excitons. The states with spin $S_{\rm exc}=0,\pm 1$ are optically active. They can be created through unpolarized optical excitation. Those with $S_{\rm exc}=\pm 1$ can be selectively created through circularly polarized optical excitation. The states with $S_{\rm exc}=0$ are created by linearly polarized (in the x or y direction) optical excitation.

III. RESULTS AND DISCUSSIONS

The system we consider here is a GaAs quantum well of thickness L embedded in semiinfinite layers of $Ga_{0.7}Al_{0.3}As$. The parameters used in the calculations are $m_e=0.067m_0$, $\gamma_1=6.85$, $\gamma_2=2.1$, $\gamma_3=2.9$, $\kappa=13.8$, and $Q_e=0.6$. Once we are dealing with the solutions of the coupled-exciton system, there no longer exists the well-defined heavy- and light-hole excitons, even at $\vec{K}_{\rm c.m.}=0$. Nevertheless, for the sake of language simplicity, we continue to call them as heavy- and light-hole excitons.

A. Exciton center-of-mass dispersion

In Fig. 1 we show the in-plane dispersions for the first two exciton states $e_1-hh_1{:}1s$ and $e_1-lh_1{:}1s$ for a well width

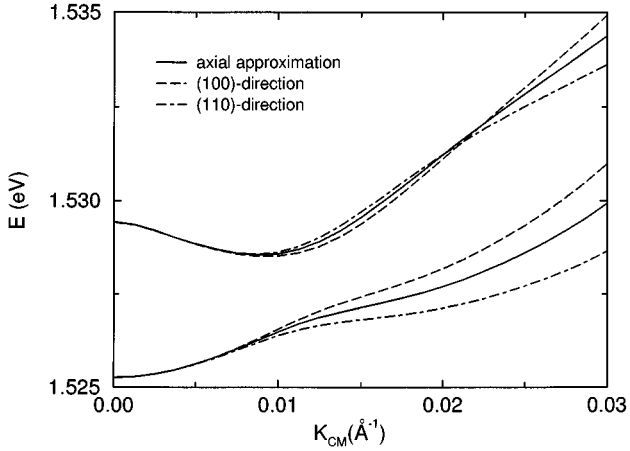

FIG. 1. Exciton-c.m. dispersion for $L=200$ Å GaAs/$Ga_{0.7}Al_{0.3}As$ quantum well. Solid lines, axial approximation; dashed lines, (100) direction; dash-dotted lines, (110) direction.

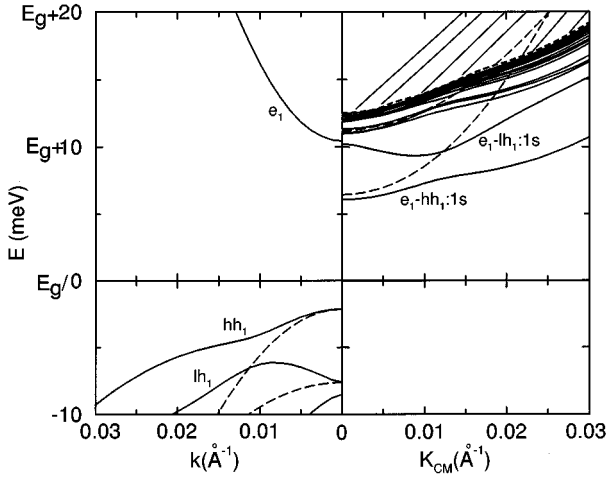

FIG. 2. Hole subband and exciton-c.m. dispersions for the same QW as in Fig. 1. Solid lines, coupled excitons; dashed lines, uncoupled approximation. The shaded area represents the excitonic continuum states.

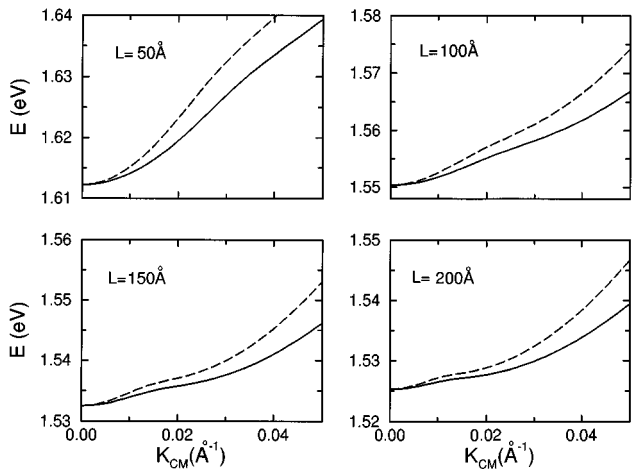

FIG. 3. Comparison between exciton and hole subband dispersions for several $GaAs/Ga_{0.7}Al_{0.3}As$ QW widths. Solid lines, fundamental exciton dispersion; dashed lines, first heavy-hole subband dispersion (shifted to coincide with the exciton $K_{\mathrm{c.m.}}=0$ energy).

of $L=200$ Å. Dashed and dash-dotted lines are the results in the (100) and (110) in-plane directions, respectively, while the solid lines are the results in the axial approximation. The results show that, as is the case for the hole dispersions,[15] the axial approximation well describes the average value of the in-plane dispersions and the warping in the dispersion can be neglected in a first approximation. From now on, we use only the axial approximation in our calculations.

Figure 2 shows both the electron and hole subband dispersions and the exciton-c.m. dispersions for the first states for the same QW as in Fig. 1. In the left-hand side, we plot the conduction- and valence-subband dispersions. The right-hand side shows the exciton-c.m. dispersion. The zero of energy is chosen at the top of the GaAs bulk valence band for the subband dispersion, while the exciton energy scale represents the total exciton energy. The dashed lines are the dispersions in the uncoupled valence-subband approximation, when the off-diagonal terms of the Luttinger Hamiltonian are set equal to zero. Only the $e_1-hh_1:1s$ and $e_1-lh_1:1s$ exciton states are shown in this approximation. The solid lines display the results obtained using the full exciton Hamiltonian [Eq. (3)]. For this well width the $e_1-lh_1:1s$ exciton is below the e_1-hh_1 exciton continuum and is a true bound state. Some excited exciton states are also shown. The dotted line is the threshold of the exciton continuum and the shaded area represents the exciton continuum.

The first remarkable feature is the strong nonparabolicity of the exciton-c.m. dispersion. The valence-subband mixing features are mainly transferred to the exciton dispersion. This behavior for the in-plane c.m. dispersion is expected since the c.m. motion is dominated by the heavier mass ($M_{\mathrm{exc}}=m_e+m_h$). An important feature is the camel-back shape of the $e_1-lh_1:1s$ exciton. This is a reminescence of a similar feature in the light-hole dispersion. This may affect several properties of the exciton. It should present poor luminescence, which could, in principle, only take place through phonon-assisted emission. This favors its relaxation to the ground heavy-hole exciton. Also, its heavy in-plane mass may favor its localization in defects as it diffuses along the plane of the QW. For QW widths narrower than 160 Å, the $e_1-lh_1:1s$ exciton degenerates with the continuum of the e_1-hh_1 exciton and it becomes a resonance, with most of these effects being smoothed out. An interesting case was study by Michler *et al.*[31] They considered the $In_{1-x}Ga_xAs/InP$ system. For samples with a Ga concentration higher than 47%, the $In_{1-x}Ga_xAs$ is under tension. As the Ga concentration rises, the $e_1-lh_1:1s$ state approaches the $e_1-hh_1:1s$ state until it becomes the ground exciton state. In the process, the camel-back structure is transferred to the ground exciton state and the system shows a poor luminescence. Michler *et al.*[31] observed that the luminescence lifetime increases in two orders of magnitude, demonstrating the indirect nature of the ground exciton state in the samples with the appropriate Ga concentration. This result was predicted by Chu and Chang[39] and it was confirmed in our previous calculations.[41]

The exciton dispersion follows, in a good approximation, the hole subband dispersion. The parabolic dispersion of the conduction subband smooths the excitonic nonparabolic dispersion. This is better observed in Fig. 3 where we plot the ground hole subband and the ground exciton state dispersions for QW widths $L=50$, 100, 150, and 200 Å. For better comparison, the hole dispersion is shifted in energy to coincide with the exciton dispersion at $\vec{K}_{\mathrm{c.m.}}=0$. We clearly observe that the exciton has, in average, a heavier mass and its nonparabolicity is slightly smoothed out in comparison to the hole subband dispersion.

In Fig. 4 we show the fundamental heavy-hole exciton dispersion and some of the higher-energy states for several QW widths. In this figure, the solid lines are the coupled-exciton dispersion and the dashed lines are the uncoupled (parabolic) approximation. We observe that the increase of the well width enhances the nonparabolicity of the exciton dispersion, induced by the increasing of the coupling among the excitonic states. The c.m. wave vector value of the anticrossing decreases as the QW width increases. For $L=150$ Å the $e_1-lh_1:1s$ exciton is still in the e_1-hh_1 continuum. As $K_{\mathrm{c.m.}}$ increases, the initially $e_1-hh_1:2s$ state

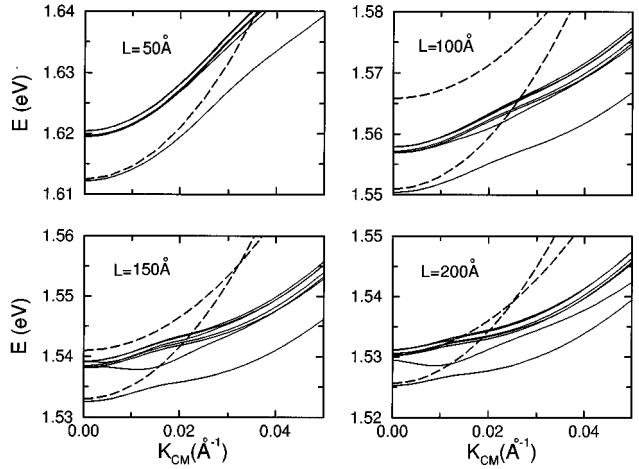

FIG. 4. Exciton-c.m. dispersions for several $GaAs/Ga_{0.7}Al_{0.3}As$ QW widths. Solid lines, coupled excitons; dashed lines, uncoupled approximation.

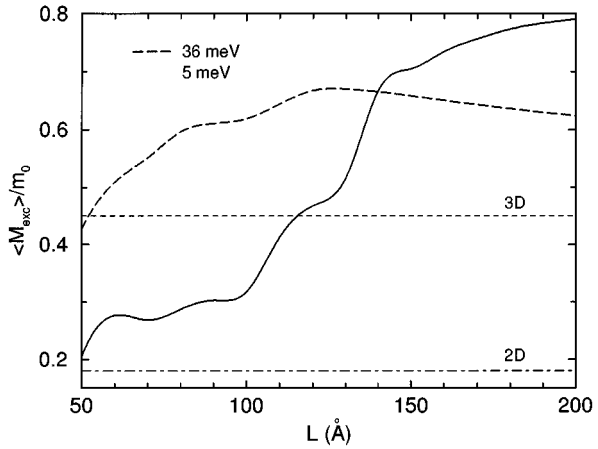

FIG. 5. Average exciton effective mass as a function of the GaAs QW width. The average is obtained from a parabolic fit of the fundamental exciton dispersion, within two energy ranges: 5 meV (solid line) and 36 meV (dashed lines). The bulk value (dotted line) and the uncoupled 2D limit (dot-dashed line) are also shown.

(the second state in energy at $K_{\text{c.m.}}=0$) acquires a dominant $e_1-lh_1:1s$ character and shows the camel-back structure. For $L=200$ Å the $e_1-lh_1:1s$ exciton is a true bound state, showing the same feature. A comparison with the valence-subband dispersion (not shown here) shows that the camel-back profile on the exciton-c.m. dispersion appears for QW widths larger than those for the light-hole subband dispersion.

The process of formation of excitons is still not clear.[24–27] Two paths are possible. The electron-hole pair is created at high energies. (i) They may relax toward their subband edges through phonon emission and then scatter with acoustic phonons, forming an exciton with a finite c.m. wave vector. In this case, the exciton kinetic energy will be lower than the exciton binding energy. The exciton will then relax towards the bottom of the exciton dispersion through acoustical phonons emission. (ii) The exciton may also be rapidly formed once the electron-hole pair is created. The excitons would then have a large kinetic energy and large c.m. wave vector. They will first rapidly relax toward the exciton bottom of band through LO-phonon emission and then through acoustical-phonon emission along the exciton-c.m. dispersion branch. The acoustical-phonon emission starts when the exciton has an energy not higher than the LO-phonon energy ($\sim$36 meV). Both processes are accompanied by exciton diffusion along the QW plane. As a consequence, the exciton may also be trapped in alloy fluctuations or interface roughnesses. This process is strongly dependent on the exciton mass. As we showed here, this value is dependent on the c.m. wave vector since the exciton-c.m. dispersion is highly nonparabolic. However, some insight into the exciton mobility may be obtained through its average mass. Figure 5 shows the average values for the effective mass of the fundamental exciton as a function of the well width. The average effective masses were obtained from a parabolic fit of the excitonic dispersion curves. The results represent an average value for states within a certain range of energy. The solid line shows the mass averaged in an energy range of 5 meV. This value is approximately the exciton kinetic energy after it is formed from an electron and a hole which first relaxed to the bottom of the subbands. The dashed line shows the exciton average mass calculated in a range of energy of 36 meV and corresponds to the excitons after they emitted LO phonons once they were formed from hot electron-hole pairs. The dashed and dot-dashed lines are the uncoupled 3D and 2D exciton mass values. For average over 5 meV, the exciton average mass is more sensitive to the dispersion nonparabolicity. For low QW's it shows a light mass, near the uncoupled in-plane exciton mass, $M_{\text{c.m.}}\sim m_e+m_0/(\gamma_1+\gamma_2)=0.18m_0$. For a QW width of $L\sim100$ Å, it shows a sharp increase in the average mass and starts to saturate near $L\sim150$ Å with the average mass reaching values as high as $M_{\text{c.m.}}\sim0.8m_0$, which is well above the bulk value, $M_{\text{c.m.}}=m_e+m_0/(\gamma_1-2\gamma_2)=0.45m_0$. The increase in the average mass is related to the coupling with the $e_1-lh_1:1s$ exciton which depends on the hole subband energy separation. The exciton mass averaged over the energy range of 36 meV shows a smoother dependence with the QW width. In this case, the coupling between the excitons is included in the average already at narrow wells. The average mass reaches a maximum of $M_{\text{c.m.}}\sim0.67m_0$ near $L\sim130$ Å and converges towards the bulk values for larger QW's. These results give some indication of the possibility of exciton trapping while it relaxes. For instance, there is a larger probability of the excitons being trapped in narrow QW's since in this case the electron-hole wave functions have a larger probability at the interface and the barrier than for larger QW widths. However, if the excitons are formed with low kinetic energy, they will show a light mass, which favors their mobility and lowers the probability of being trapped. A complete description of the exciton dynamics and relaxation requires a time-dependent solution of the coupled exciton in the presence of the scattering centers.

B. Electric-field effects

We consider now the effects of an external longitudinal electric field. In this case, there is no more bound states in the QW. However, the QW barrier potential allows for the existence of quasidiscrete QW bound states, that is, strong resonances capable of withstanding large fields.[49] It is pos-

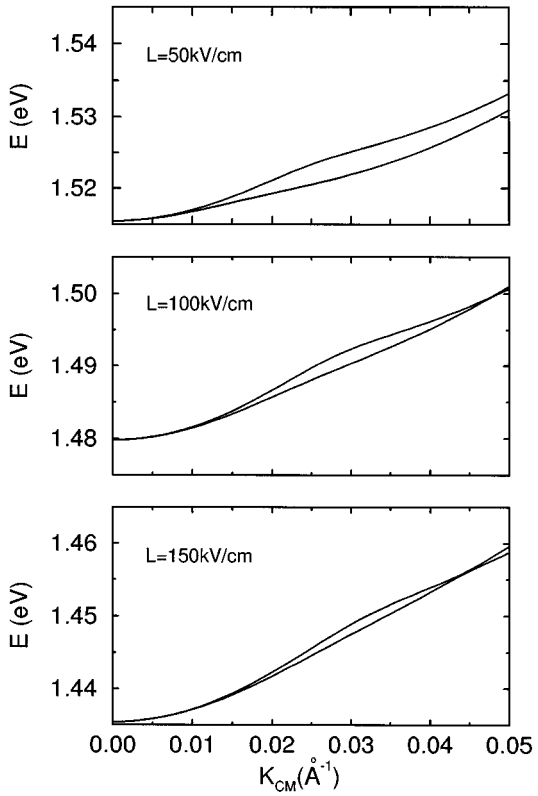

FIG. 6. Ground exciton dispersions for a 150-Å-thick $GaAs/Ga_{0.7}Al_{0.3}As$ QW in the presence of an external electric field.

sible to achieve large Stark shifts while still observing strong excitonic like absorption peaks.[50] The electric field polarizes the electron and the hole to different directions of the QW. However, the exciton still shows a strong binding energy.[51] The single-particle QW Stark shift is proportional to the carrier mass. The energy separation between the heavy-hole and light-hole subbands can then be controlled through the application of the electric field. This effect was used to demonstrate the coupling among heavy- and light-hole excitons with different in-plane symmetries.[18,19]

The longitudinal electric field breaks the mirror symmetry in respect to the center of the QW. As a consequence, the degeneracy in the hole subband dispersions is lifted. Figure 6 shows the ground-exciton-c.m. dispersion for a QW width $L=150$ Å and electric fields $F=50$, 100, and 150 kV/cm. We clearly observe the break of the degeneracy at finite values of $K_{\text{c.m.}}$. The effect is, however, weaker for electric fields larger than 50 kV/cm. This is a consequence of two competing effects: Large electric fields enhance the asymmetry in the QW, but also increase the energy separation between the ground heavy- and light-hole subbands, diminishing the effects of the coupling among the exciton states. For the parameters considered here, the latter effect dominates and the break of the degeneracy is more noticeable for $F=50$ kV/cm than for $F=150$ kV/cm. Note that both dispersions converge to the same value at $K_{\text{c.m.}}=0$, as it should be, since the electric field does not lift the degeneracy at the center of the zone.[19] Figure 7 shows the average exciton effective mass for the two branches of the dispersion as a function of the electric field. The difference between the two average masses can be larger than 50%. They converge to

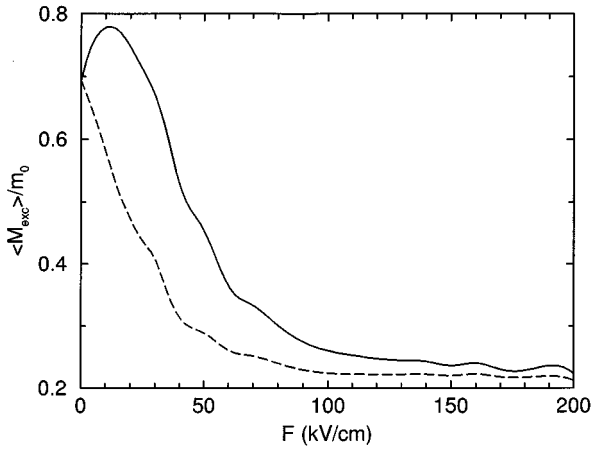

FIG. 7. Average excitonic effective mass as a function of external electric field for the same exciton as in Fig. 6. The average is obtained from a parabolic fit of the exciton dispersion within an energy range of 5 meV. Solid line, lower-energy dispersion; dashed line, higher-energy dispersion.

the same value as the electric field increases. Except for one of the branches at small electric fields, the average mass decreases with the field as a consequence of the increasing in the energy separation between the heavy- and light-hole ground subbands. The average masses converge to a value slightly above the uncoupled in-plane exciton mass. The average masses give just an insight for the exciton dynamics. The two dispersion branches are actually coupled and during the scattering processes the exciton can switch from one branch to the other.

C. Exciton spin

The coupling among the exciton states induces a strong mixing in the exciton spin. It is this mixing that allows for the exciton spin relaxation. Figure 8 shows the average spin $\langle S_{\text{exc}}\rangle$ as defined in Eqs. (26) and (27) as a function of $\vec{K}_{\text{c.m.}}$ for two directions of the exciton dispersion for the same QW as in Fig. 1, for the $e_1-hh_1{:}1s$ and $e_1-lh_1{:}1s$ exciton states. Here the in-plane dispersion warping was in-

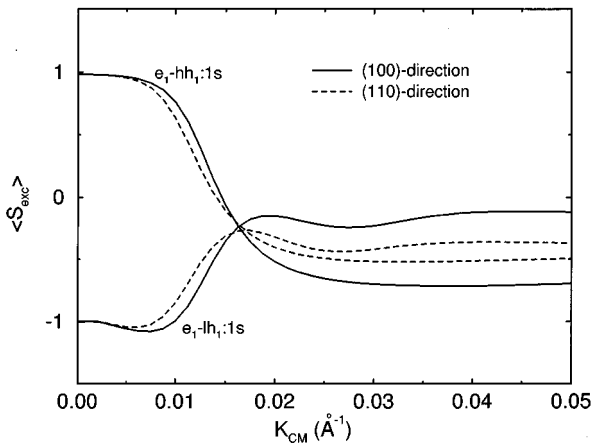

FIG. 8. Average excitonic spin as a function of $K_{\text{c.m.}}$ for the $e1-hh1{:}1s$ and $e1-lh1{:}1s$ excitonic states. Solid lines, (100) direction; dashed lines, (110) direction. $L=200$ Å.

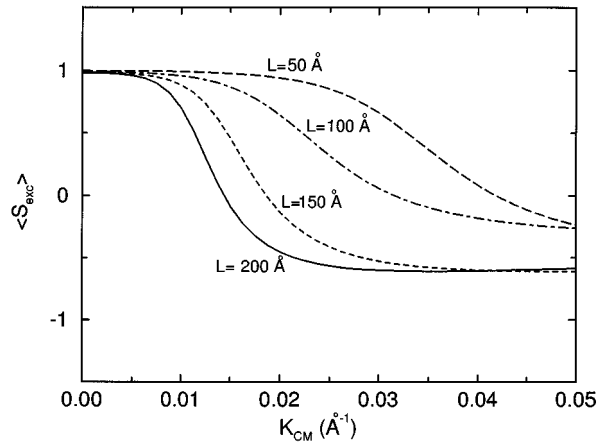

FIG. 9. Average spin of the ground exciton state for several QW widths in the axial approximation.

cluded. The others spin mixings [Eqs. (24) and (25), (28) and (29), and (30) and (31)] show the same pattern. Although there is a mixing already at $\vec{K}_{\text{c.m.}}=0$, this is a very small effect. Most of the mixing starts at the anticrossing value of $\vec{K}_{\text{c.m.}}$. This corresponds to a kinetic energy of only ~ 1.5 meV for the ground exciton state. The exciton spin becomes completely blurred at $K_{\text{c.m.}}>0.0154$ Å^{-1}. Figure 9 shows $\langle S_{\text{exc}}\rangle$ as a function of $K_{\text{c.m.}}$ for different values of the QW width in the axial approximation. As expected, the strong mixing in the exciton spin occurs for lower values of $K_{\text{c.m.}}$ as the QW width increases. This difference is more important if we consider the equivalent exciton kinetic energy (see Fig. 3). For $L=50$ Å the strong spin mixing starts for an exciton kinetic energy of ~ 20 meV while for $L=200$ Å the exciton is already strongly mixed at energies of ~ 2 meV. Because of the coupling, the exciton flips its spin as it relaxes and reaches the bottom of its dispersion. Since excitons, electron, and holes relax their spin with different rates, the spin relaxation is strongly dependent on the exciton creation process. The QW width plays a fundamental role as well, since, depending on the mechanism for the exciton creation and on the QW width, the exciton may be created in a state already strongly mixed or not. This ''initial condition'' for the exciton relaxation certainly influences the final outcome of the entire process. For a more complete analysis of the exciton spin relaxation, it is necessary to include the exchange interaction[32] in our calculation. Although this interaction is weak, it is responsible for the coupling among different exciton states and is fundamental in the process of the exciton spin flip.[32]

IV. CONCLUDING REMARKS

We presented here the results of the calculation of the exciton c.m. dispersion. The excitons show similar features as the holes in their dispersion. In particular, we observe that the parabolic electron mass does not smooth out the camelback shape of the dispersion. The exciton in-plane mass and the average spin are strongly dependent on the exciton kinetic energy as well as the QW width. Our calculations are a first step in understanding the effects of the valence-subband coupling in the exciton dynamics. This allows us to calculate several processes, like the exciton spin relaxation and exciton formation and relaxation, including exciton mixing in a nonperturbative way.

ACKNOWLEDGMENTS

We gratefully acknowledge financial support from CNPq (Brazil) and FAPESP (Brazil).

[1] R. J. Elliot, Phys. Rev. **108**, 1384 (1957).
[2] M. D. Sturge, Phys. Rev. **127**, 768 (1962).
[3] G. Livescu, IEEE J. Quantum Electron. **24**, 2677 (1988).
[4] M. Altarelli and N. O. Lipari, Phys. Rev. B **15**, 4898 (1977).
[5] Al. L. Éfros and B. L. Gelmont, Solid State Commun. **49**, 883 (1984).
[6] B. L. Gelmont, S. B. Sultanov, and Al. L. Éfros, Sov. Phys. Semicond. **18**, 1380 (1984).
[7] G. Wannier, Phys. Rev. **52**, 191 (1937).
[8] G. Dresselhaus, J. Phys. Chem. Solids **1**, 14 (1956).
[9] D. A. B. Miller, D. S. Chemla, D. J. Eilenberger, P. W. Smith, A. C. Gossard, and W. T. Tsang, Appl. Phys. Lett. **41**, 679 (1982).
[10] G. Bastard, *Wave Mechanics Applied to Semiconductor Heterostructures* (Les Editions de Physique, Les Ulis, 1989).
[11] H. W. Liu, R. Ferreira, G. Bastard, C. Delalande, J. F. Palmier, and B. Etienne, Appl. Phys. Lett. **54**, 2082 (1989).
[12] G. Bastard, J. A. Brum, and R. Ferreira, in *Solid State Physics*, edited by H. Ehrenreich and Turnbull (Academic, New York, 1991), Vol. 44.
[13] R. L. Greene and K. K. Bajaj, Solid State Commun. **45**, 831 (1983).
[14] J. A. Brum and G. Bastard, J. Phys. C **18**, L789 (1985).
[15] M. Altarelli, in *Heterojunctions and Semiconductor Superlattices*, edited by G. Allan, G. Bastard, N. Boccara, M. Lannoo, and M. Voos (Springer-Verlag, Berlin, 1986), and references therein.
[16] K. S. Chan, J. Phys. C **19**, L125, (1986).
[17] G. E. W. Bauer and T. Ando, Phys. Rev. B **38**, 6015 (1988).
[18] L. Viña, R. T. Collins, E. E. Mendez, and W. I. Wang, Phys. Rev. Lett. **58**, 832 (1987).
[19] G. E. W. Bauer and T. Ando, Phys. Rev. Lett. **59**, 601 (1987).
[20] L. Viña, G. E. W. Bauer, M. Potemski, J. C. Maan, E. E. Mendez, and W. I. Wang, Phys. Rev. B **38**, 10 154 (1988); Phys. Rev. Lett. **59**, 602 (1987).
[21] J. A. Brum, P. Hiergeist, G. Abstreiter, J. P. Reithmaier, and H. Riechert, in *Europhysics Conference Abstracts*, 12th General Conference of the Condensed Matter Division of the E.P.S., Praha, 1992, edited by B. Veilcký, V. Vonlicek, and K. Záveta (Union of Czechoslovak Mathematicians and Physicists, Praha, 1992).
[22] R. C. Miller, D. A. Kleinman, W. T. Tsang, and A. C. Gossard, Phys. Rev. B **24**, 1134 (1981).
[23] C. Weisbuch, R. Dingle, A. C. Gossard, and W. Wiemann, Solid State Commun. **38**, 7091 (1981).
[24] T. C. Damen, J. Shah, D. Y. Oberli, D. S. Chemla, J. E. Cunningham, and J. M. Kuo, Phys. Rev. B **42**, 7434 (1990).
[25] B. Deveaud, F. Clérot, N. Roy, K. Satzke, B. Sermage, and D. S.

Katzer, Phys. Rev. Lett. **67**, 2355 (1991).
[26] Ph. Roussignol, C. Delalande, A. Vinattieri, L. Carraresi, and M. Colocci, Phys. Rev. B **45**, 6965 (1992).
[27] R. Khumar, A. S. Vengurlekar, S. S. Prabhu, J. Shah, and L. N. Pfeiffer, Phys. Rev. B **54**, 4891 (1996).
[28] C. Weisbuch, M. Nishioka, A. Ishikawa, and Y. Arakawa, Phys. Rev. Lett. **69**, 3314 (1992).
[29] R. Houdré, R. P. Stanley, U. Oesterle, M. Ilegems, and C. Weisbuch, J. Phys. (France) IV **3**, 51 (1993).
[30] S. Jorda, Phys. Rev. B **50**, 2283 (1994).
[31] P. Michler, A. Hangleiter, A. Moritz, G. Fuchs, V. Härle, and F. Sholz, Phys. Rev. B **48**, 11 991 (1993).
[32] M. Z. Maialle, E. A. Andrada e Silva, and L. J. Sham, Phys. Rev. B **47**, 15 776 (1993).
[33] A. Vinattieri, J. Shah, T. C. Damen, D. S. Kim, L. N. Pfeiffer, M. Z. Maialle, and L. J. Sham, Phys. Rev. B **50**, 10 868 (1994).
[34] J. Kusano, Y. Segawa, Y. Aoyagi, S. Namba, and H. Okamoto, Phys. Rev. B **40**, 1685 (1989).
[35] A. Zrenner, L. V. Butov, M. Hagn, G. Abstreiter, G. Bhöm, and G. Weimann, Phys. Rev. Lett. **72**, 3382 (1994).
[36] G. D. Gilliland, A. Antonelli, D. J. Wolford, K. K. Bajaj, J. Klem, and J. A. Bradley, Phys. Rev. Lett. **71**, 3717 (1993).
[37] M. A. Cotta, R. A. Hamm, T. W. Staley, S. N. G. Chu, L. R. Harriot, M. B. Panish, and H. Temkin, Phys. Rev. Lett. **70**, 4106 (1993).
[38] R. Nötzel, Semicond. Sci. Technol. **11**, 1365 (1996).
[39] H. Chu, G. D. Sanders, and Y. C. Chang, Phys. Rev. B **36**, 7955 (1987).
[40] X. R. Resende and J. A. Brum, IL Nuovo Cimento **170**, 1675 (1995).
[41] A. L. C. Triques and J. A. Brum, in *Proceedings of the 22th International Conference on Physics of Semiconductors*, Vancouver, Canada, 1994, edited by D. J. Lockwood (World Scientific, Singapore, 1995), Vol. 2, p. 1328.
[42] J. M. Luttinger, Phys. Rev. **102**, 1030 (1956).
[43] U. Ekenberg and M. Altarelli, Phys. Rev. B **35**, 7585 (1987).
[44] U. Fano, Phys. Rev. **124**, 1866 (1961).
[45] J. A. Brum and D. Y. Oberli, J. Phys. (France) IV Colloq. **C5**, C5-191 (1993).
[46] D. Y. Oberli, G. Böhm, G. Weimann, and J. A. Brum, Phys. Rev. B **49**, 5757 (1994).
[47] J. A. Brum, D. Y. Oberly, and A. L. C. Triques, in *Current Topics in Quantum Electronics*, edited by J. Menon (Kaithamukku, Trivandrum, India, 1994), Vol. 1, pp. 139–156.
[48] D. Broido and L. J. Sham, Phys. Rev. B **31**, 888 (1985).
[49] G. Bastard, E. E. Mendez, L. L. Chang, and L. Esaki, Phys. Rev. B **28**, 3241 (1983).
[50] T. H. Wood, C. A. Burrus, D. A. B. Miller, D. S. Chemla, T. C. Damen, A. C. Gossard, and W. Wiemann, Appl. Phys. Lett. **44**, 16 (1984).
[51] J. A. Brum and G. Bastard, Phys. Rev. B **31**, 3893 (1985).